Journal of Alloys and Compounds 501 (2010) 317–325

Contents lists available at ScienceDirect

Journal of Alloys and Compounds

journal homepage: www.elsevier.com/locate/jallcom

Size and crystallinity-dependent magnetic properties of copper ferrite nano-particles

N.M. Deraz

Chemistry Department, College of Science, King Saud University, P.O. Box 2455, Riyadh 11451, Saudi Arabia

ARTICLE INFO

Article history:
Received 21 December 2009
Received in revised form 7 April 2010
Accepted 14 April 2010
Available online 22 April 2010

Keywords:
Copper ferrite nano-particles
Crystallinity
Crystallite and particle size
Saturation and remanence magnetization
Coercivity

ABSTRACT

Copper ferrite nano-crystals were synthesized by a combustion route depending upon the glycine–nitrate process and also by ceramic method. In order to investigate the effect of degree of crystallinity and crystallite size of copper ferrite system on its magnetic properties, a series of Cu-ferrite samples with different degrees of crystallinity and crystallite size were produced by varying the preparation temperatures via changing the ratio between the glycine and nitrates. The samples were characterized by infrared radiation (IR), X-ray diffraction (XRD), scanning electron micrograph (SEM), transmission electron micrograph (TEM) and vibrating sample magnetometer (VSM) techniques. The IR and XRD patterns confirm the single-phase spinel structure for the synthesized materials. Transmission electron microscopy analysis revealed needle-like tubular nanostructures containing polygon particles. VSM investigations showed that the saturation magnetization of the Cu-ferrite possessed a linear relationship with both crystallinity and crystallite size.

1. Introduction

The preparation and functionalization of nano-structured magnetic materials has been an interesting area of study because of its possible applications in a variety of widely diversified areas ranging from information technology to nano-biotechnology [1]. Among magnetic materials, spinel ferrites of the type $M^{2+}Fe_2^{3+}O_4$ (M = Mn, Mg, Zn, Ni, Co, Cd, etc.) attract the research interest because of their versatile practical applications such as electric motors, electric guitar pickups, loudspeakers, automotive and electronic sensors, actuators, hall effect sensors, magnetron, reed switches, TWT amplifiers, communication, vehicle signage, shelf and bin marking, craft, hobby, toys, industrial automation equipment, transformers, rotating transformers, pulse transformers, catalysts and adsorptive materials [2–5].

The preparation method plays a very important role with regard to the chemical and structural properties of the spinel ferrite [6–11]. In fact, the diverse available methods or routes to prepare nano-ferrites that have been published, such as ball-milling [9–13], sol–gel and co-precipitation [10,14–16] and ceramic synthesis [17], are interesting and attract much research attention.

However, these preparation methods are generally complicated and expensive especially when organo-metallic precursors and complex process controls are involved. Sol–gel techniques involve the use of large amounts of organic solvents to the reaction medium. It is far from being environmentally friendly. In a co-precipitation procedure, the pH of a metal salt solution is raised by adding a base in order to precipitate the hydroxides; this requires a strict control of the pH and the stirring rate. The ball-milling method and ceramic synthesis are unfavourable to make ferrite at low cost, because of the problems such as the complex process and high-energy consumption.

Deraz reported that the Mn_2O_3 or CuO interacted readily with ferric oxide at temperatures starting from 700 or 800 °C for 5 h yielding $MnFe_2O_4$ or $CuFe_2O_4$, respectively. The degree of propagation of $MnFe_2O_4$ or $CuFe_2O_4$ formation increased as a function of calcination temperature of the mixed solids investigated [18,19]. Srivastava et al. reported that nano-composites containing spinel and CuO phases have been synthesized by sol–gel method using Cu(II), Ni(II) and Fe(III) in a basic medium [20]. Authors indicated that the increase in the calcination temperature led to an increase in the values of the saturation magnetization, remanent magnetization and coercivity of the nano-composites depending upon the particle size. The effect of preparation method on the surface properties and activity of $Ni_{0.7}Cu_{0.3}Fe_2O_4$ nano-particles was studied [11]. These nano-particles were synthesized via sol–gel combustion technique, co-precipitation method and solid state milling method. The investigators revealed that simultaneous thermo-gravimetric and differential thermal analyses of the precursors show that the crystallization temperature for spinel formation by sol–gel combustion technique is lower than that by co-precipitation method and solid state milling method. XRD analysis reveals that the powders obtained had a single phase with cubic spinel structure. The

E-mail address: nmderaz@yahoo.com.

0925-8388/$ – see front matter © 2010 Elsevier B.V. All rights reserved.
doi:10.1016/j.jallcom.2010.04.096

experimental study of these particles indicates that the copper in the octahedral sites plays a crucial role in the direct oxidation of benzene with hydrogen peroxide as oxidant to phenol [11].

A novel preparation technique of nano-materials, combustion synthesis has been developed to prepare nano-sized compounds [21–23]. Combustion synthesis (CS) or self-propagating high-temperature synthesis (SHS) is an effective, low-cost method for the production of various industrially useful materials. Today, CS has become a very popular approach for the preparation of nano-materials and it is practised in 65 countries. Recently, a number of important breakthroughs in this field have been made, notably for the development of new catalysts and nano-carriers with properties better than those for similar traditional materials. The extensive research carried out in the past 5 years emphasized the SHS capabilities for material improvement, energy saving and environmental protection [23]. The importance of industrialization of the SHS process was also realized.

Deraz et al. had prepared various ferrites, $MnFe_2O_4$, $NiFe_2O_4$ and $ZnFe_2O_4$, using combustion method [24–26]. It was concluded that the combustion route is simple, fast and inexpensive. It is easy to control the stoichiometry and crystallite size, which have an important influence on structural, morphology, magnetic and electric properties of ferrites. The effect of copper substitution on the structural and magnetic properties in $Ni_{0.7}Zn_{0.3}Fe_2O_4$ synthesized by a combustion method was determined [27]. The results revealed that increasing amounts of copper brought about a decrease in the saturation magnetization and the Curie temperature values. This decrease was explained in terms of the magnetic moments and magnetic exchange interactions existing between the anti-parallel uncompensated electron spin of tetrahedral and octahedral sub-lattices involved in the spinel structure. However, the nearly constant lattice parameters obtained with Cu substitution were attributed to the small difference in the ionic radius between Ni^{2+} and Cu^{2+} ions.

Because copper ferrite ($CuFe_2O_4$) is one of the important ferrites [12], the magnetic behaviour of $CuFe_2O_4$ has been the much interesting subject of intensive studies [13,15]. In this context, $CuFe_2O_4$ assumes great significance because of its high electronic conductivity, high aluminium stability and high catalytic activity of O_2 evolution from alumina–cryolite system used for that it serves as a non-consumable and green anode for aluminium electrolysis. The significance is that at $CuFe_2O_4$ anode, only oxygen gas is evolved instead of CO_2—a green house gas at the widely used carbon anode [28].

The combustion technique brings a good chance to study $CuFe_2O_4$ nano-particle. In this paper, $CuFe_2O_4$ nano-particles were prepared by this simple low heating solid state reaction. One of our aims was to develop a general synthetic method and explore the magnetic properties of the $CuFe_2O_4$ nano-particles. Furthermore, investigation of the fuel-cation ratio effect on the crystallite size, particle size, lattice constant, unit cell volume, X-ray density and the saturation of magnetization of the as-prepared copper ferrite. Finally, we compared the different properties of the as-prepared Cu-ferrite to those of the bulk copper ferrite.

2. Experimental

2.1. Materials

Series of copper ferrite samples were prepared by mixing calculated proportions of copper and iron nitrates with different amounts of glycine. The mixed precursors were concentrated in a porcelain crucible on a hot plate at 300 °C for 5 min. The crystal water was gradually vaporized during heating and when a crucible temperature was reached, a great deal of foams were produced and spark appeared at one corner which spread through the mass, yielding a voluminous and fluffy product in the container. In our experiments, the ratio of the glycine:copper nitrate:ferric nitrate was (0, 2, 4, 6 and 8):1:2 for C1, C2, C3, C4 and C5 samples, respectively.

Additional sample (C6) for bulk copper ferrite was prepared by ceramic process involving high-temperature (1000 °C for 5 h) solid state reaction between the reacting constituents as shown in our last work [18]. The chemicals employed in the present work were of analytical grade supplied by Prolabo Company. It had been reported that the ratio of glycine to nitrates (G/N) had a strong impact on the experimental temperature and also a higher G/N ratio would lead to a higher temperature [25].

2.2. Techniques

An X-ray measurement of various mixed solids was carried out using a BRUKER D8 advance diffractometer (Germany). The patterns were run with Cu Kα radiation at 40 kV and 40 mA with scanning speed in 2θ of 2° min^{-1}.

The crystallite size of Cu-ferrite present in the investigated solids was based on X-ray diffraction line broadening and was calculated by using Scherrer equation [29]:

$$d = \frac{B\lambda}{\beta\cos\theta} \quad (1)$$

where d is the average crystallite size of the phase under investigation, B is the Scherrer constant (0.89), λ is the wave length of X-ray beam used, β is the full-width half maximum (FWHM) of diffraction and θ is the Bragg's angle.

An infrared absorbance spectrum of various solids was determined using Perkin-Elmer Spectrophotometer (type 1430). The IR spectra were determined from 1000 to 300 cm^{-1}. Two milligrams of each solid sample were mixed with 200 mg of vacuum-dried IR-grade KBr. The mixture was dispersed by grinding for 3 min in a vibratory ball mill and placed in a steel die 13 mm in diameter and subjected to a pressure of 12 tonnes. The sample disks were placed in the holder of the double grating IR spectrometer.

Scanning electron micrographs (SEMs) and transmission electron micrographs (TEMs) were recorded on JEOL JAX-840A and JEOL JEM-1230 electron micro-analyzers, respectively. The samples were dispersed in ethanol and then treated ultrasonically in order to disperse individual particles over gold grids.

The magnetic properties of the investigated solids were measured at room temperature using a vibrating sample magnetometer (VSM; 9600-1 LDJ, USA) in a maximum applied field of 15 kOe. From the obtained hysteresis loops, the saturation magnetization (M_s), remanence magnetization (M_r) and coercivity (H_c) were determined.

3. Results

3.1. FTIR analysis

The formation of the spinel $CuFe_2O_4$ structure in the nano-crystalline form was supported by infrared spectra. These spectra were recorded in the range 300–1000 cm^{-1}, which is shown in Fig. 1. The spectra show two main absorption bands γ_1 and γ_2 corresponding to the stretching vibration of the tetrahedral and octahedral sites around 600 and 400 cm^{-1}, respectively. The observed values illustrate that the frequency bands appearing at 545–568 and at 410–467 cm^{-1} are responsible for the formation of $CuFe_2O_4$ [18]. The bands γ_1 and γ_2 are shifted from lower band values to higher band values due to the shifting of Fe^{3+} and Cu^{2+} ions towards oxygen ion on occupation of tetrahedral and octahedral sites by increasing the G/N ratio with subsequent increase on the Fe^{3+}–O^{2-} and Cu^{2+}–O^{2-} distances [28]. However, the FTIR spectrum shows a subsidiary band at 387–396 cm^{-1} for all the investigated solids. This may be due to Fe^{2+} oxygen complexes in octahedral site. The presence of Fe^{2+} ion causes the splitting of absorption bands due to local lattice deformation. It is seen from the spectra of $CuFe_2O_4$ prepared using combustion route that there is shoulder for the tetrahedral site band located at 688 cm^{-1}. It is attributed to the presence of lower ionic states in that site, i.e. diffusion of Cu^{2+} by the replacement of Fe^{3+} in the A-site. In addition, a close scrutiny of A-site frequency indicates that there is a progressive increase in the value of frequency when compared to its bulk counterpart. It explains the expansion of bond length for that site [28]. A possible interpretation is that the larger Cu^{2+} ions (0.069 nm) diffuse into A-site replacing the native ions Fe^{3+} (0.064 nm).

It can be seen that the Cu^{2+} ions which otherwise have the tendency to occupy octahedral site tend to occupy tetrahedral site also. But the percentage of Cu^{2+} ions occupying octahedral site is

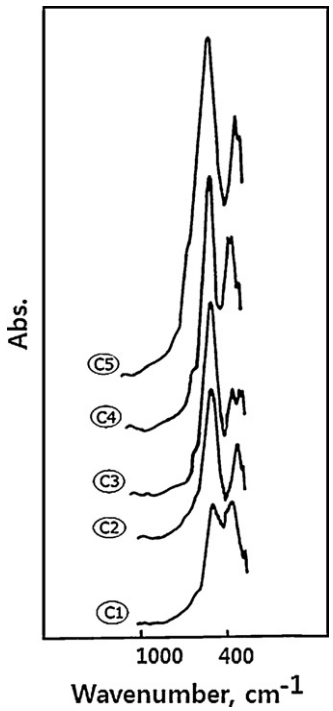

Fig. 1. FTIR spectra of the C1, C2, C3, C4 and C5 samples.

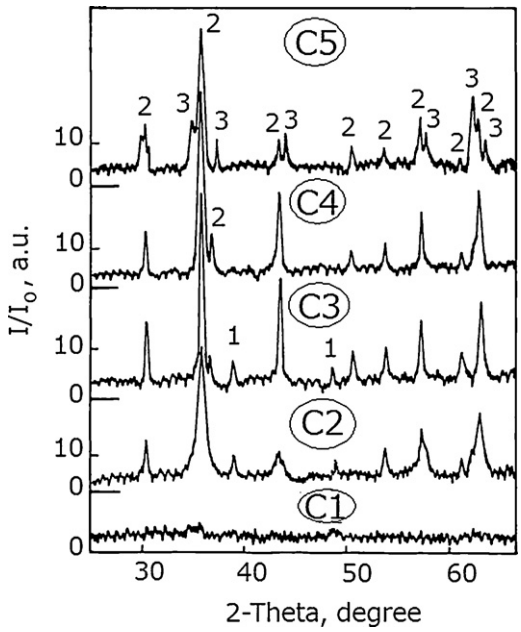

Fig. 2. X-ray diffraction patterns of the C1, C2, C3, C4 and C5 samples; lines (1) CuO, (2) cubic $CuFe_2O_4$ and (3) tetrahedral $CuFe_2O_4$ phases.

comparatively greater for the as-prepared samples. Therefore, any distortion in the structure is caused by the migration of more number of Cu^{2+} ions to the tetrahedral site during combustion process. On the basis of the above data, the copper ferrite compound has a partially inverse spinel structure and the cation distribution is as follows:

$$(Cu_x{}^{2+}Fe^{3+})_A[Cu_{1-x}{}^{2+}Fe^{3+}Fe^{2+}]_BO_4{}^{2-} \quad (2)$$

This indicates that the presence of glycine as fuel enhances the formation of copper ferrite. In other words, the increase of the G/N ratio resulted in a progressive increase in the formation of copper ferrite phase that was proportional to the amount of glycine added. Since the weight of mixed solids was constant in each IR run, the area of various peaks for the different solids could be looked as a measure of the amount of solid undergoing a chemical change. Inspection of the IR spectra of the different investigated solids reported that addition of the increasing amount of glycine led to an increase in the area of all investigated peaks to an extent proportional to the amount of glycine added. This indicates an increase in the amount of the as-prepared copper ferrite and stimulation of the thermal decomposition of copper and iron nitrates in the presence of glycine as fuel. This treatment brought about an increase in a solid state reaction between Cu/Fe mixed oxides and/or phase transformation process of one of the resulted products. These findings will be confirmed later by XRD measurements.

3.2. Structural characterization

The recorded XRD patterns of C1, C2, C3, C4 and C5 solid samples are shown in Fig. 2. Inspection of this figure revealed that: (i) The C1 sample consisted of amorphous solid which has not been detected by XRD technique. This may be indicating a possible formation of copper, iron oxides and/or copper ferrite ($CuFe_2O_4$) in amorphous state. (ii)The C2 and C3 specimens consisted of well crystalline $CuFe_2O_4$ phase (major phase) and trace amount of CuO, indicating the promotion effect of glycine as fuel in the conversion of most Cu and Fe oxides to produce copper ferrite crystallites. (iii) Increasing amounts of glycine brought about complete conversion of un-reacted oxides to well crystalline copper ferrite as the single phase with cubic spinel structure as shown in the C4 and C5 samples. This means that the rise in the G/N ratio from 0.67 to 2 led to an important increase in both the amount of the librated gases and the peaks height of cubic $CuFe_2O_4$ crystallite suggesting an increase in the amount of this phase. Similar result was observed in the case of the bulk sample (C6) related to the formation of cubic $CuFe_2O_4$ phase but with higher crystallite size of 125 nm [18]. Moreover, the augmentation in the G/N ratio above this limit resulted in partial conversion in the spinel structure from cubic to tetrahedral form. In fact, when the G/N ratio is 2.67, there are extra peaks which are identified as tetrahedral $CuFe_2O_4$ peak with subsequent decrease in the peak height of cubic Cu-ferrite phase [26]. (iv) The rise in the G/N ratio brought about a progressive shift of the diffraction peaks of $CuFe_2O_4$ to higher Bragg's angle indicating the enhancement formation of copper ferrite. In addition, the intensities of the (2 2 0) and (4 0 0) or (4 4 0) planes are more sensitive to the cations on tetrahedral and octahedral sites, respectively [28]. As reported earlier Cu^{2+} ions have a strong preference to occupy B sites [18]. Table 1 shows the observed intensities of the above three planes. It can be observed that the intensities of the (4 0 0) or (4 4 0) planes increase with the addition of glycine as fuel, which infers that the Cu^{2+} has preferentially occupied the B site, i.e. the octahedral site on the (4 0 0) or (4 4 0) planes. However, the intensity of (2 2 0) plane increases slightly by the continuous addition of glycine indicating the preferential occupation of A sites by Fe^{3+} ions.

Since the $CuFe_2O_4$ is established to be an inverse spinel structure. X-ray data enable us to investigate the role of the G/N ratio

Table 1
The effects of the G/N ratio on the intensity values of *h k l* planes of $CuFe_2O_4$ phase.

Solids	G/N ratio	Peak height (a.u.)		
		I_{220}	I_{400}	I_{440}
C2	0.67	11	7	17
C3	1.33	12	21	18
C4	2.00	13	22	22
C5	2.67	12	10	20

Table 2
Some structural parameters of copper ferrites.

Solids	G/N ratio	Crystallinity ($d_{2.52}$, a.u.)	Crystallite size (nm)	Lattice constant (nm)	Volume (nm^{-3})	Density (g/cm^3)
C2	0.67	34	14	0.8374	0.5872	5.4127
C3	1.33	40	39	0.8388	0.5895	5.3911
C4	2.00	46	42	0.8396	0.5918	5.3701
C5	2.67	37	22	0.8375	0.5875	5.4094

in modifying the structural parameters such as the crystallite size (D), lattice constant (a), unit cell volume (V) and X-ray density (D_x) for the produced copper ferrite crystallites. The calculated values of different structural parameters are given in Table 2. It can be seen from this table that the rise in the G/N ratio brought about an increase in the values of a, D and V. However, this treatment led to a decrease in the density of copper ferrite compound. In addition, the crystallinity and crystallite size of bulk copper ferrite sample (C6) synthesized by ceramic method are greater than those of $CuFe_2O_4$ crystallites prepared by combustion route [18].

3.3. Morphology and microstructure

The typical SEM of samples C1, C2, C3 and C5 are shown in Fig. 3a–d. As can be seen, the powders basically consist of equiaxial particles as shown in the sample C1. It shows that the samples C2, C3 and C5 are spongy and porous agglomerates. Voids and holes can be seen, which result from the escape of gases during combustion. By SEM observations, it was found that as the G/N ratio was increased, the porosity of the resultant powders also increased due to the evolution of more produced amounts of gas. The pressure exercised by gaseous species should be responsible for the break-up of the porous structure and the coalescence between particles leading to a surface homogeneity (Fig. 3d).

Our previous study on SEM analysis of bulk copper ferrite (C6) sample reported that the C6 sample consists of agglomerated grains with visible grain boundaries. The grain size distribution is very heterogeneous with well-crystallized grains. Also, TEM image of C6 specimen showed a relatively heterogeneous grain distribution consisting of bamboo-like tubular nanostructures, with an average grain size of 125 nm.

Transmission electron micrographs (TEMs) of the as-prepared copper ferrite and the selected area electron diffraction (SAED) pattern are shown in Figs. 4 and 5. It indicates that the copper ferrite particles obtained by combustion method are uniform in both morphology and crystallite size, but having agglomeration to some extent, due to interaction between magnetic particles and the enormous heat generated during the combustion process. The TEM image of the C1 sample exhibits very dense agglomerates as shown in Fig. 4a. When the G/N ratio is 1.33, Fig. 4b–e, the grain size distribution is very homogeneous with well-crystallized grains with visible grain boundaries. In other words, the C3 sample, with different magnifications, shows needle-like tubular nanostructures containing polygon particles. Increasing the G/N ratio above this limit brought about slight agglomeration of the as-prepared particles with formation of the ellipsoid shapes (Fig. 4f). It seems that the enormous heat liberated during the combustion process is sufficient for the crystallization of the desired ferrite phase with a

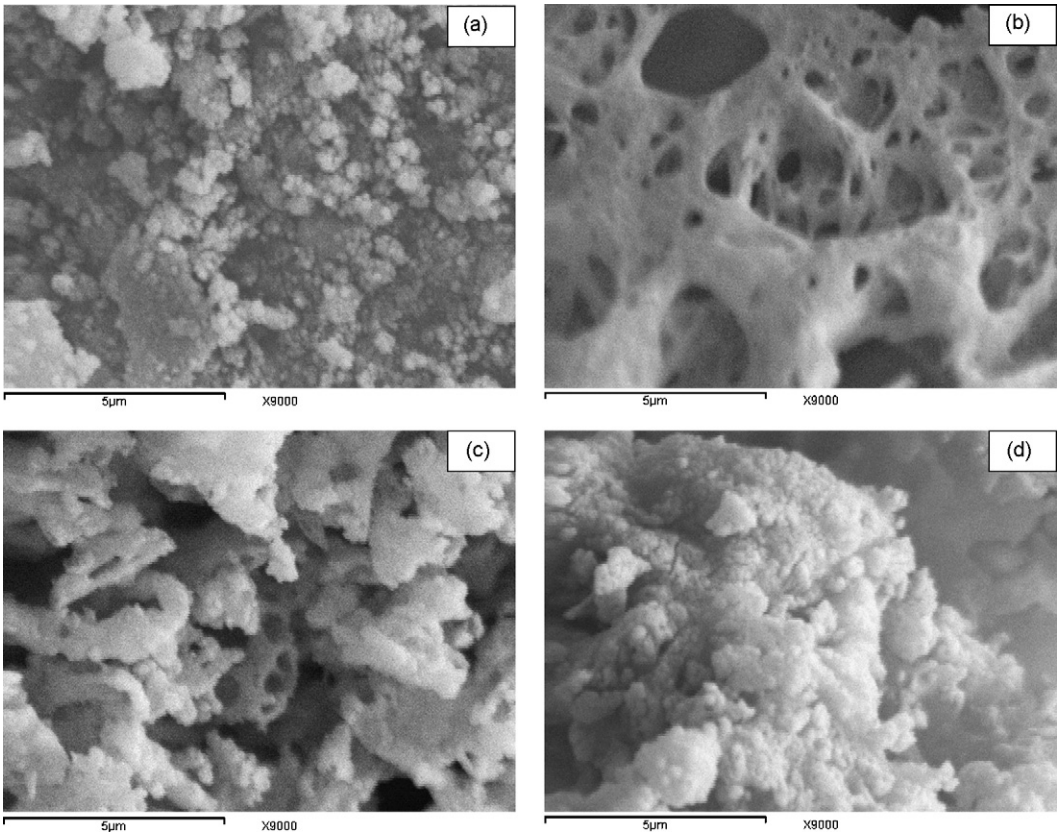

Fig. 3. SEM images of the samples: (a) C1, (b) C2, (c) C3 and (d) C5.

subsequent significant modification in its particle size. From the TEM images, the average grain sizes of obtained samples could be estimated as 10–40 nm, which are consistent with the results obtained from XRD patterns according to the Scherrer formula. By adjusting the glycine to nitrite ratio, we can control the reaction temperature, and thereby control both the crystallinity and crystallite size of the resultant system. Our results indicate that the lower G/N value leads to the smaller crystallite size with a subsequent decrease in the degree of crystallinity of the copper ferrite produced. It is interesting to observe from these figures that the average grain size is saturated as the G/N ratio increased in the range of 0.67–2.67. The increase in grain sizes and the change in grain boundary nature upon combustion process are likely to be responsible for the observations of the XRD peaks in the final products.

The SAED of some samples reveals the ring patterns of polycrystalline cubic spinel ferrite phase and the uniformity of the spinel ferrite in the samples as shown in Fig. 5a–c. The spotty nature of the SAED pattern can be due to the fact that the finer crystallites having related orientations are agglomerated together resulting in a limited set of orientations. The diffraction rings correspond to the *d*-spacing values of the spinel copper ferrite phase and the lattice parameters are in agreement with the XRD patterns. Moreover, Fig. 5a–c shows continuous rings with increasing spots which indicate an increase in the amount of $CuFe_2O_4$ crystallites involved in the as-prepared solids. It is interesting to observe the diffraction rings in the case of the sample C1, Fig. 5a, which did not show any XRD peak. These rings show that this sample consists of micro-crystalline copper ferrite which was not detected in the X-ray diffraction study. The d_{hkl} values of the diffraction rings for the as-prepared powders were calculated using the Bragg's condition applicable to electron diffraction [30]. These values could be indexed to a spinel copper ferrite phase. From the XRD and TEM study, it has been observed that the degree of agglomeration is low in the synthesized powders, which has strong technological importance.

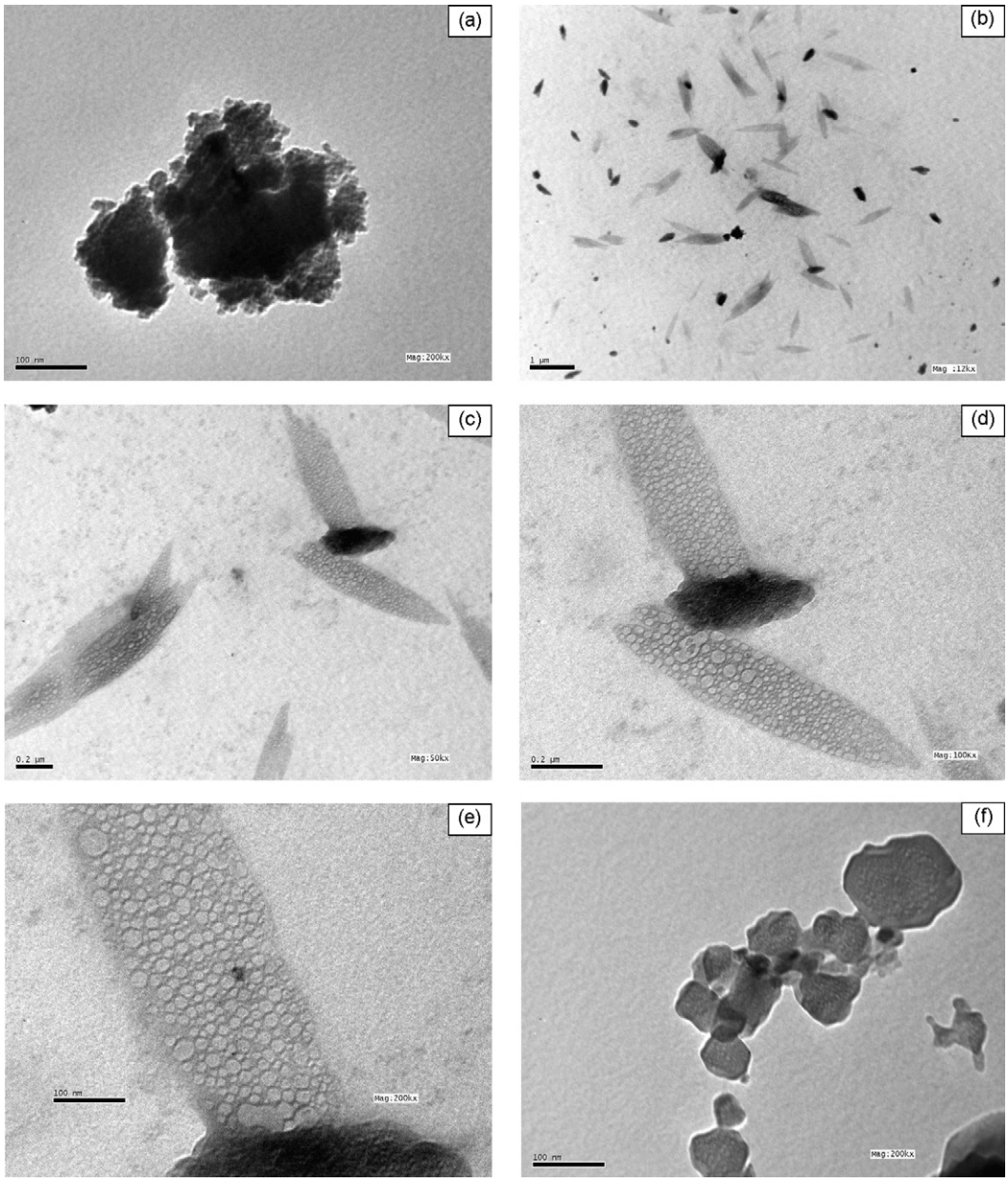

Fig. 4. TEM images of the samples: (a) C1, (b–e) C3 with different magnifications and (f) C5.

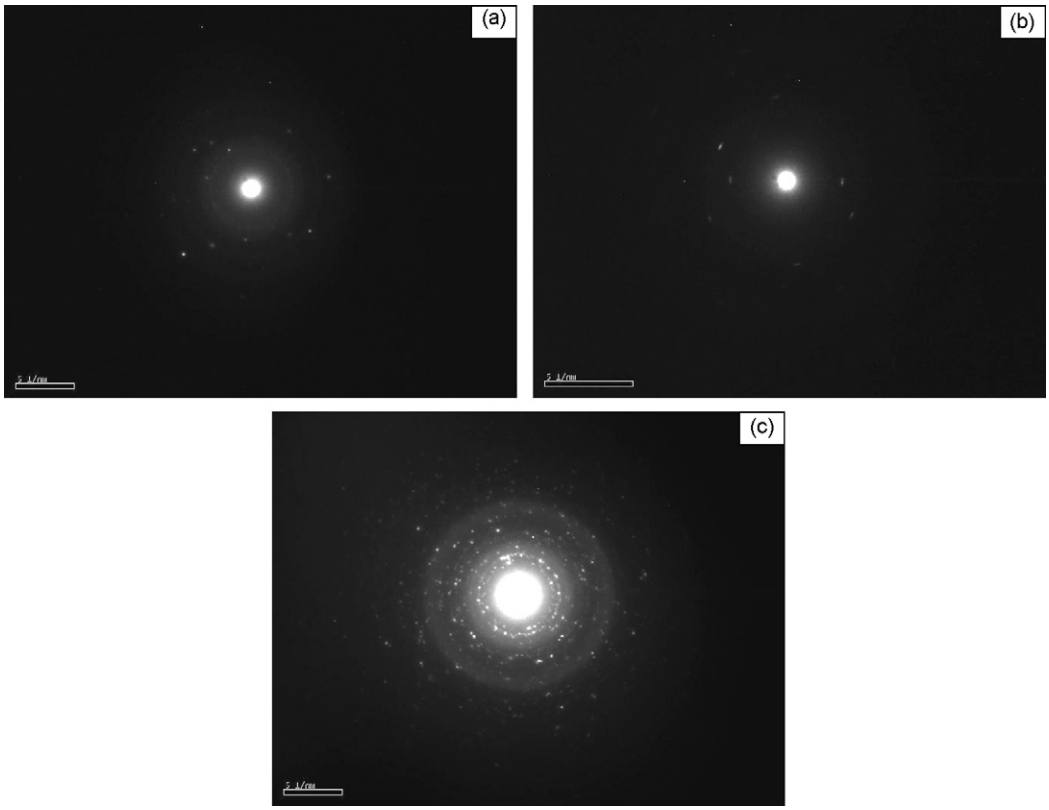

Fig. 5. SAED images of the samples: (a) C1, (b) C2 and (c) C5.

3.4. Magnetic properties

The magnetic properties measured by vibrating sample magnetometer at room temperature for Cu-ferrite samples are listed in Table 3. Fig. 6a–f shows the magnetic hysteresis curves in a magnetic field of 15 kOe of the samples synthesized by the glycine–nitrate process and also of bulk copper ferrite specimen. For all prepared samples except the C1 specimen, the hysteresis loops obtained show a normal *S*-shape type, the size and shape of hysteresis curves for a magnetic material are of considerable practical importance. The 'thickness' of the middle bit of the *S*-shaped loop describes the amount of hysteresis, related to the coercivity of the material. The width and the degree of constriction of hysteresis loop systematically vary with the increase of the G/N ratio. The C2 sample with lowest G/R ratio shows constricted loop with the medium width (Fig. 6b); the loop is suggestive of a significant content of ferromagnetic materials. Constriction appears pronounced for samples with intermediate values of G/N ratio (Fig. 6c and d). This hysteresis loop is narrower especially at the middle of the loop and results in constricted shape which is largely suppressed. The C5 sample with high G/R ratio shows slightly constricted loops with the largest width (Fig. 6e). These distorted hysteresis loops originate from mixed assemblage of multiple magnetic components with different grain sizes.

Table 3
The magnetic properties (M_s, M_r and H_c) of the as-prepared Cu/Fe mixed oxide solids.

Solids	G/N ratio	M_s (emu/g)	M_r (emu/g)	M_r/M_s (emu/g)	H_c (Oe)
C1	0.00	0.575	0.012	0.0212	132
C2	0.67	19.04	3.891	0.2044	131
C3	1.33	48.05	9.303	0.1936	76
C4	2.00	49.00	11.97	0.2440	97
C5	2.67	33.66	11.77	0.3476	28.5
C6	0.00	50.00	12.85	0.2570	95

It can be seen from Table 3 that the saturation magnetization, M_s, and remnant magnetization, M_r, vary as a function of the G/N ratio. It can be observed that the values of M_s and M_r were increased by increasing the G/N ratio from 0 to 2, and then were decreased above this limit, whereas the coercivity decreases with this ratio, then increases. The M_s and M_r values show their maximum around the G/N ratio of 2. These values are near from that of the bulk copper ferrite sample (C6) as shown in Table 3. On the other hand, the coercivity shows rather complicated dependency on the G/N ratio. The coercivity of the investigated solids displays its maximum at a G/N ratio of 2.67. From the hysteresis loops, the ratio *R* of the remnant to the saturation magnetization (M_r/M_s) is derived to determine whether the inter- and intra-grain exchange interactions, sub-lattice magnetization, magnetic anisotropy and morphology of the sample exist [31,32]. The augmentation in the G/N ratio resulted in a significant increase in the value of *R*. The changes in the magnetic properties of the samples can be attributed to the crystallite size and crystallinity, depending on the G/N ratio [25–28,33].

4. Discussion

Some of the physical and chemical methods widely used in the synthesis of nano-ferrites are ceramic, ball-milling, sol–gel, co-precipitation, spray pyrolysis and hydrothermal methods [18,34–38]. As compared with the conventional synthesis methods, the combustion route is observed to be a high yielding and low-cost route. The final nano-sized bulk product is thus obtained without sophisticated equipment. Earlier works have reported the need for calcination of Cu/Fe mixed oxides at higher temperatures for yielding copper ferrite and improving the phase purity and crystallinity [18,39]. Though the combustion route yields more promising results in the synthesis of nano-ferrites [18,28,40], several preparation conditions such as dilution, fuel/oxidant ratio, pH

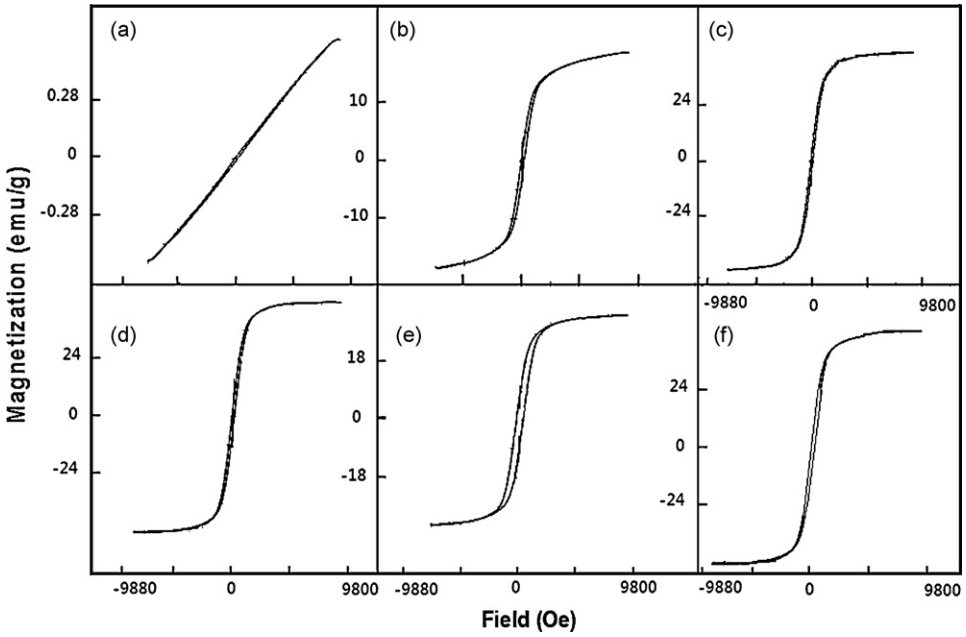

Fig. 6. Magnetic hysteresis curves measured at a room temperature for the samples: (a) C1, (b) C2, (c) C3, (d) C4, (e) C5 and (f) C6.

and temperature can have an impact on the formation of the ferrites and their properties [41]. In the present work a sincere attempt is made to change the fuel/oxidant ratio of the precursor solution used in combustion route of synthesis to produce the single $CuFe_2O_4$ particles and study the impact of nano-regime on the structural, morphological and magnetic parameters.

Glycine is considered to serve as fuel for the combustion reaction, being oxidized by nitrate ions. Stoichiometrically balanced [42], the exothermic reaction can be expressed as:

$$18Fe(NO_3)_3 + 9Cu(NO_3)_2 + 32NH_2CH_2COOH + 54O_2 \rightarrow 9CuFe_2O_4 + 16N_2 + 72NO_2 + 64CO_2 + 80H_2O$$

It had been reported that the ratio of glycine to nitrates (G/N) had a strong impact on the experimental temperature [43]. In other words, a higher glycine to nitrate ratio would lead to a higher reaction temperature [20]. It seems that the enormous heat liberated during the combustion process is sufficient for the crystallization of the desired ferrite phase. Moreover, the temperature reached in the combustion reaction has an important effect on the crystallinity and crystallite size of the powder resultants. By adjusting the G/N ratio, we can control the reaction temperature, and thereby control the degree of crystallinity and crystallite size of the resultants. The XRD pattern of $CuFe_2O_4$ powder consists of well-resolved peaks characteristic of polycrystalline spinel phase. The formation of better crystalline and face centred cubic structure may be due to the enormous heat generated during the combustion of large amount of glycine present in the precursor. The propagation of the solid state reaction between iron and copper oxides is controlled by thermal diffusion of Cu and Fe cations through the ferrite film which covers the surfaces of grains of reacting oxides and acts as energy barrier. The fact is that the increase in the G/N ratio brought about an increase in the extent of the produced $CuFe_2O_4$ phase. When the G/N ratio of the precursor solution is much lower than the stoichiometrical ratio, the diffraction peaks of the samples are broadened. In addition, the full-width at half-maxima (FWHM) of the peaks decreases with an increase in the G/N ratio. The average size of the crystallites can be estimated from the FWHM of the peaks using the Scherrer equation, and the results are listed in Table 2. Our results in Table 2 indicate that the lower G/N value leads to the smaller crystallite size and vice versa depending upon the heat liberated during the combustion process [28]. Increasing the crystallite size of the as-prepared solids could be attributed to the slightly coalescence between the nano-particles as shown in SEM and TEM investigations (Figs. 3d and 4f). This confirms by increasing the volume of unit cell and lattice constant of the as synthesized ferrite via increasing the G/N ratio. The resultant nano-scaled crystallite size of samples is owing to two characteristics of the reaction system. One is that the reactants have been uniformly dispersed at an atomic or molecular level before reaction, so when ignition occurred, the nucleation process can be completed through only the rearrangement and short-distance diffusion of nearby atoms. The other is that the rate of combustion reaction is so high that enough time and energy are not provided for the long-distance diffusion of atoms and obvious growth of the crystallites, as a result of which, the initial nano-phase is retained.

As mentioned earlier, our TEM study showed that the increase in grain sizes and the change in grain boundary nature upon changing the G/N ratio are likely to be responsible for the observation of the XRD peaks in the investigated samples. Also, the change in the G/N ratio brought about a phase transition tetragonal-to-cubic structure of the as-prepared copper ferrite. A close scrutiny of the XRD pattern of the different samples shows a slight distortion in the cubic structure which is understood from the peaks observed at (2 2 0) and (4 0 0) reflection planes. The intensities of the (2 2 0) and (4 0 0) planes are more sensitive to the cations on tetrahedral and octahedral, respectively [28,44–46]. It can be observed from Table 1 that the intensity of the (4 0 0) plane increases with the increase of the G/N ratio up to 2, which implies that the Cu^{2+} ions have preferentially occupied the B site with a subsequent replacement of Fe^{3+} by Cu^{2+} ions. The maximum increase in the intensity of the (4 0 0) planes attained 214%. This observation confirms the significant increase in both the crystallite size and lattice constant of the copper ferrite due to the expansion of ferrite lattice depending upon the ionic radii of Fe^{3+} by Cu^{2+} ions were 0.064 and 0.069 nm, respectively. In fact, the Cu^{2+} ions which otherwise have the tendency to occupy octahedral site tend also to occupy tetrahedral site. The rise in the G/N ratio up to 2.67 resulted in a decrease in both the crystallite size and lattice constant of the copper ferrite from 42 and 0.8396 to 22 and 0.8375 nm, respectively. This is referred to migration of

some Fe^{3+} and Cu^{2+} from A and B sites to B and A sites, respectively, confirming a phase transition cubic to tetragonal structure of the $CuFe_2O_4$ crystallites. Indeed, it is seen from Fig. 2 that the rise in the G/N ratio led to a progressive increase in the peak height of lines at *d*-spacing 0.25 nm relative to tetragonal copper ferrite form and a decrease in that at *d*-spacing 0.252 nm characteristic of cubic copper ferrite form (major phase). This might refer to the transformation of some cubic phase into tetragonal phase [12]. Moreover a rapid cooling which may occur statistically at some regions of the nano-particles might have caused an average and minor distortion [47].

The changes in the structural and morphological properties of the as synthesized ferrite resulted in some modifications in their magnetic properties. The magnetic order of copper ferrite is related to the inter-granular coupling due to a large fraction of grain boundary volume present in the powders. The grain boundary regions are an array of dislocations in the material [48]. Thus, the "effective" grain size could be much larger. The augmentation in the preparation temperature leads to an increase in the grain size with a subsequent decrease in the grain boundary volume depending upon reduce the volume fraction of high angle grain boundary. This can also be explained by the kinetics of the grain boundary [48]. The low angle grain boundaries are less mobile compared with high angle grain boundaries, and therefore, may not collapse even at high preparation temperatures. Hence, it is expected that the low angle grain boundaries would be present even when the powders are heated at high temperatures leading to an inhibition of grain growth at a particular temperature. It is concluded that the observed magnetic behaviour in the powders can be ascribed to inter-granular coupling between grains via low angle grain boundaries.

The structural properties of copper ferrite affect their magnetic properties depending on the sizes of crystallites. Our results show that the saturation magnetization and remnant magnetization values of the samples increase with increasing particle sizes which arise from spin non-colinearity at the surface of the crystals while the coercivity field values have no similar orderliness. The energy of a magnetic particle in the external field is proportional to its particle sizes via the number of molecules in a single magnetic domain. Therefore, the decrease in the values of M_s and M_r with the decrease of particle sizes can be attributed to surface effects that are the result of finite-size scaling of nano-crystallites [49]. Indeed, the lower M_s and M_r values for the sample C5 associated with the particles with smaller size could be attributed to two factors. First, surface distortion due to the interaction of transition metal ions with the oxygen atoms in the spinel lattice can reduce the net magnetic moment in the particle. This effect is especially prominent for the ultra-fine particles due to their large surface to volume ratio [50]. Second, the magneto-crystalline anisotropy of the particles is dependent on the degree of the crystallinity of the nano-particles. A large proportion of crystal defects and dislocations can occur within the lattice of the sample C5. This will cause a significant reduction of the magnetic moment within the particles as a result of the magneto-crystalline anisotropy distortion.

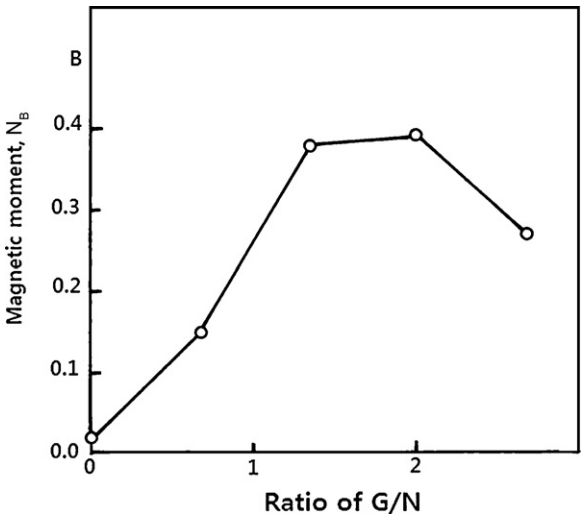

Fig. 7. Variation of magnetic moments of the investigated solids with the G/N ratio.

Indeed, the experimental values of the magnetic moment (N_B) expressed in Bohr magnetron are determined and illustrated in Fig. 7. This figure shows the relation between the magnetic moment and the G/N ratio. It can be seen from this figure that the increase in the G/N ratio up to 2 led to an increase in the magnetic moment then it decreased by increasing the G/N ratio above this limit. The change in the magnetic moment could be attributed to A–B interaction and migration of some copper ions in copper ferrite depending on the presence of non-collinear arrangement on the B sub-lattice which is reflected in magnetization measurements due to the randomly canted structure present in ferrite system. However, increasing the G/N ratio up to 2.67 resulted in the partial conversion of cubic copper ferrite phase to its tetragonal form depending on frozen of part of the Cu^{2+} ions in tetrahedral sites. Close to thermodynamic equilibrium at room temperature, the copper ferrites may be described by the structural formula $Fe^{3+}[Fe^{3+}Cu^{2+}]O_4^{2-}$, in which the octahedral cations are placed inside square brackets. The spinel lattice is thus highly distorted because of a cooperative Jahn–Teller effect arising from the octahedral cupric ions [51]. Part of the Cu^{2+} ions can be frozen in tetrahedral sites when the ferrites are quenched in air from temperatures higher than 400 °C [29]. The resulting ferrites show a smaller tetragonal distortion since a great proportion of the cupric ions are located on tetrahedral sites. Finally, Cu-ferrite powders can be stabilized in either tetragonal or cubic phase even at room temperature depending on nature and conditions of preparation process [7,12,15,18,52–57]. This study revealed that the $CuFe_2O_4$ crystallites can be stabilized in cubic phase with the G/N ratio in the range of 0.67–2 and also stabilized in mixture of cubic and tetrahedral phases above this limit.

5. Conclusions

We have successfully prepared nano-crystalline Cu-ferrites with tunable magnetic properties. The influence of the preparation temperature, via changing the ratio between glycine and nitrates (G/N), on the magnetic properties and crystallite size of the ferrite samples synthesized by the combustion method was investigated with the aim of tuning the magnetic properties and greatly expanding the range of applications. Our results showed that this method facilitates the magnetic tunability of the Cu-ferrite nano-particles by using the proper the G/N ratio. The Cu-ferrite samples obtained by this method had the single-phase spinel structure and good magnetic properties. The magnetic properties of the ferrite samples were strongly affected by the G/N ratio as a consequence of the gradual increase in the crystallinity and particle size. Particle sizes of the samples increased with the G/N ratio. The magnetization values of the samples increase with the increase of the particle sizes. This observation is more pronounced for the sample containing a single cubic copper ferrite when the G/N ratio has the value of 2. On the other hand, the combustion method displays magnetic copper ferrite in the range of nano-scale comparing of bulk ferrite prepared by ceramic route.

References

[1] D. Bahadur, J. Giri, B.B. Nayak, T. Sriharsha, P. Pradhan, N.K. Prasad, K.C. Barichk, R.D. Ambashta, J. Phys. 65 (2005) 663.
[2] M. Sugimoto, J. Am. Ceram. Soc. 82 (1999) 269.
[3] K. Raj, B. Moskowitz, R. Casciari, J. Magn. Magn. Mater. 149 (1995) 174.
[4] R.D. McMichael, R.D. Shull, L.J. Swartzendruber, L.H. Bennett, R.E. Watson, J. Magn. Magn. Mater. 111 (1992) 29.
[5] Z. Sun, L. Liu, D.Z. Jia, W. Pan, Sens. Actuators B 125 (2007) 144.
[6] X. Tan, G. Li, Y. Zhao, C. Hu, J. Alloys Compd. 493 (2010) 55.
[7] D. Gingasu, I. Mindru, L. Patron, C.-B. Cizmas, J. Alloys Compd. 460 (2008) 627.
[8] Z.G. Zheng, X.C. Zhong, Y.H. Zhang, H.Y. Yu, D.C. Zeng, J. Alloys Compd. 466 (2008) 377.
[9] Y. Choi, N.I. Baik, J. Alloys Compd. 466 (2009) 134.
[10] M.R. Barati, J. Alloys Compd. 478 (2009) 375.
[11] M. Sinha, S.K. Pradhan, J. Alloys Compd. 489 (2010) 91.
[12] G.F. Goya, H.R. Rechenberg, Nanostruct. Mater. 10 (1998) 1001.
[13] J.Z. Jiang, G.F. Goya, H.R. Rechenberg, J. Phys. Condens. Mater. 11 (1999) 4063.
[14] P.B. Pandya, H.H. Joshi, R.G. Kulkarni, J. Mater. Sci. Lett. 10 (1991) 474.
[15] C. Despax, P. Tailhades, C. Baubet, C. Villette, A. Rousset, Thin Solid Films 293 (1997) 22.
[16] S.W. Tao, F. Gao, X.Q. Liu, O. Toft Sørensen, Mater. Sci. Eng. B77 (2000) 172.
[17] Y.S. Zhang, G.C. Stangle, J. Mater. Res. 9 (1994) 1997.
[18] N.M. Deraz, J. Anal. Appl. Pyrol. 82 (2008) 212.
[19] N.M. Deraz, Thermochim. Acta 401 (2003) 175.
[20] M. Srivastava, A.K. Ojha, S. Chaubey, P.K. Sharma, A.C. Pandey, J. Alloys Compd. 494 (2010) 275.
[21] X.R. Ye, D.Z. Jia, J.Q. Yu, X.Q. Xin, Z.L. Xue, Adv. Mater. 11 (1999) 941.
[22] Z.P. Sun, L. Liu, L. Zhang, D.Z. Jia, Nanotechnology 17 (2006) 2266.
[23] Y.L. Liu, Z.M. Liu, Y. Yang, H.F. Yang, G.L. Shen, R.Q. Yu, Sens. Actuators B 107 (2005) 600.
[24] N.M. Deraz, S. Shaban, J. Anal. Appl. Pyrol. 86 (2009) 173.
[25] A. Alarifi, N.M. Deraz, S. Shaban, J. Alloys Compd. 486 (2009) 501.
[26] N.M. Deraz, A. Alarifi, Polyhedron 28 (2009) 4122.
[27] M.A. Gabal, Y.M. Al Angari, S.S. Al-Juaid, J. Alloys Compd. 492 (2010) 411.
[28] R. Kalai Selvan, C.O. Augustin, V. Šepelák, L. John Berchmans, C. Sanjeeviraja, A. Gedanken, Mater. Chem. Phys. 112 (2008) 373.
[29] B.D. Cullity, Elements of X-ray Diffraction, Addison-Wesly Publishing Co. Inc., 1976 (Chapter 14).
[30] A.M. Glauret, Practical Methods in Electron Microscopy, vol. 1, North Holland, Amsterdam, 1972.
[31] C. Caizer, M. Stefanescu, J. Phys. D: Appl. Phys. 35 (2002) 3035.
[32] K.V.P.M. Shafi, A. Gedanken, R. Prozorov, J. Balogh, Chem. Mater. 10 (1998) 3445.
[33] Z.L. Wang, Y. Liu, Z. Zhang, Handbook of Nano-phase and Nano-structured Materials. Materials Systems and Applications I, vol. III, Kluwer Academic, Plenum Publishers, USA, 2003.
[34] S.K. Pradhan, S. Bid, M. Gateshki, V. Petkov, Mater. Chem. Phys. 93 (2005) 224.
[35] A. Pradeep, G. Chandrasekaran, Mater. Lett. 60 (2006) 371.
[36] S. Verma, P.A. Joy, Y.B. Khollam, H.S. Potdar, S.B. Deshpande, Mater. Lett. 58 (2004) 1092.
[37] S.S. Bellad, C.H. Bhosale, Thin Solid Films 322 (1998) 93.
[38] S.Z. Zhang, G.L. Messing, J. Am. Ceram. Soc. 73 (1990) 61.
[39] Y. Huang, Y. Tang, J. Wang, Q. Chen, Mater. Chem. Phys. 97 (2006) 394.
[40] Z. Yue, L. Li, J. Zhou, H. Zhang, Z. Gui, Mater. Sci. Eng. B 64 (1999) 68.
[41] L. Satyanarayana, K. Madhusudan Reddy, S.V. Manorama, Mater. Chem. Phys. 82 (2003) 21.
[42] S.R. Jain, K.C. Adiga, V. Pai Verneker, Combust. Flame 40 (1981) 71.
[43] Y. Tao, G. Zhao, W. Zhang, S. Xia, Mater. Res. Bull. 32 (1997) 501.
[44] B.P. Ladgaonkar, A.S. Vaingankar, Mater. Chem. Phys. 56 (1998) 280.
[45] C.S. Narasimhan, C.S. Swamy, Appl. Catal. 2 (1982) 315.
[46] L. John Berchmans, R. Kalai Selvan, P.N. Selva Kumar, C.O. Augustin, J. Magn. Magn. Mater. 279 (2004) 103.
[47] A.J. Pointon, J.M. Robertson, Philos. Mag. 17 (148) (1968) 703.
[48] F.J. Humphreys, M. Hatherly, Re-crystallization and Related Annealing Phenomena, Pergamon, Oxford, 1995.
[49] R.H. Kodama, A.E. Berkowitz, E.J. Mcniff, S. Foner, Phys. Rev. Lett. 77 (1996) 394.
[50] M. Rajendran, R.C. Pullar, A.K. Bhattacharya, D. Das, S.N. Chintalapudi, C.K. Majumdar, J. Magn. Magn. Mater. 232 (2001) 71.
[51] Ph. Tailhades, C. Villette, A. Rousset, J. Solid State Chem. 141 (1998) 56.
[52] C. Villette, Ph. Tailhades, A. Rousset, J. Solid State Chem. 117 (1995) 64.
[53] M. Desai, S. Prasad, N. Venkataramani, I. Samajdar, A.K. Nigam, R. Krishnan, J. Appl. Phys. 91 (2002) 2220.
[54] M. Desai, S. Prasad, N. Venkataramani, I. Samajdar, A.K. Nigam, R. Krishnan, IEEE Trans. Magn. 38 (2002) 3012.
[55] M. Desai, S. Prasad, N. Venkataramani, I. Samajdar, A.K. Nigam, R. Krishnan, J. Magn. Magn. Mater. 246 (2002) 266.
[56] D. Gingaşu, I. Mîndru, L. Patron, O. Carp, D. Matei, C. Neagoe, I. Balint, J. Alloys Compd. 425 (2006) 357.
[57] M.K. Fayek, S.S. Ata-Allah, H.A. Zayed, M. Kaiser, S.M. Ismail, J. Alloys Compd. 469 (2009) 9.